DØ Note 5392-CONF

Improved Search for Single Top Quark Production Using The Matrix Element Analysis Technique in 0.9 fb^{-1} of Data

The DØ Collaboration
URL http://www-d0.fnal.gov
(Dated: May 14, 2007)

We present an improved search for single top quarks using the matrix element analysis technique at D0 using 0.9 fb^{-1} of Run II data. It builds on the work presented in Ref. [1]. From a comparison of the matrix element discriminants between data and the background model, assuming a Standard Model cross section ratio of $\sigma_s/\sigma_t = 0.44$, we measure the single top quark production cross section:

$$\sigma\left(p\bar{p} \to tb + tqb + X\right) = 4.8^{+1.6}_{-1.4} \text{ pb}.$$

This result has a p-value of 0.08%, corresponding to a 3.2σ Gaussian-equivalent significance.

Preliminary Results for Spring 2007 Conferences

I. INTRODUCTION

The D0 Collaboration recently announced first evidence for the production of single top quarks and also the first direct measurement of $|V_{tb}|$ [1]. The analysis was based on $0.9\,\mathrm{fb}^{-1}$ of data, and used three different analysis techniques: boosted decision trees (DT), Bayesian neural networks (BNN), and the matrix element method (ME).

This note presents a second application of the ME method to the same data set. The primary change is the inclusion of a $t\bar{t}\to\ell$+jets matrix element in the three-jet bin, resulting in improved sensitivity. The reader is referred to Ref. [1, 2] for an introduction to the theory, information about the event selection, and the treatment of uncertainties.

II. SEPARATION OF SIGNAL FROM BACKGROUND USING MATRIX ELEMENTS

The matrix element method uses the matrix elements of a process to calculate the probability to observe a particular event assuming that it is the given process. The key equation is:

$$P(x|\mathrm{process}_i) = \frac{1}{\sigma_i}\frac{d\sigma_i}{dx} \tag{1}$$

where x is the configuration of the event, and $P(x|\mathrm{process}_i)$ is the probability density to observe x given that the physics process is process$_i$. More concretely, x is the set of reconstructed jet and lepton four-vectors, and possibly other information, such as b-tagging state, of the event. For each event, we can calculate $P(x|\mathrm{signal})$, which uses the matrix elements of the signal processes, and $P(x|\mathrm{background})$, which uses the matrix elements of the background processes. Bayes's Theorem then allows us to invert the relation:

$$P(\mathrm{signal}|x) = \frac{P(x|\mathrm{signal})P(\mathrm{signal})}{P(x|\mathrm{signal})P(\mathrm{signal}) + P(x|\mathrm{background})P(\mathrm{background})}. \tag{2}$$

This provides what is needed to separate signal from background: the probability that the event is signal given the event's configuration. The analysis uses a related equation:

$$D(x) = \frac{P(x|\mathrm{signal})}{P(x|\mathrm{signal}) + P(x|\mathrm{background})}. \tag{3}$$

This analysis selects events with one isolated electron or muon, missing energy, and two or three jets. One or two of those jets need to have a b-tag. For each event in each channel, two discriminant values are calculated: a t-channel discriminant and an s-channel discriminant. These discriminant values are plotted in a two-dimensional histogram, out of which a cross section is extracted using a Bayesian approach [1, 3]. Systematic uncertainties and their correlations are taken into account by integrating with Gaussian priors for each systematic uncertainty.

A. Calculation of the Event Probability Density Functions

The event configuration, x, refers to the reconstructed event configuration. However, the matrix element depends on the parton-level configuration of the event, which we will label y. The differential cross section, $d\sigma/dx$, can be related to the parton-level variant, $d\sigma/dy$, by integrating over all the possible parton values, using the parton distribution functions to relate the initial state partons to the proton and antiproton, and using a "transfer function" to relate the outgoing partons to the reconstructed objects. This is given in Eq. 4:

$$\frac{d\sigma}{dx} = \sum_j \int dy \left[f_{1,j}(q_1, Q^2)\, f_{2,j}(q_2, Q^2)\, \frac{d\sigma_{hs,j}}{dy}\, W_j(x,y)\, \Theta_{\mathrm{parton}}(y) \right] \tag{4}$$

where

- $\sum_j$ is a sum of different configurations that contribute to the differential cross section: it is the discrete analogue to $\int dy$. Specifically, it includes summing over the initial parton flavors in the hard scatter collision and the different permutations of assigning jets to partons.
- $\int dy$ is an integration over the phase space:

$$\int dy = \int dq_1 dq_2 d^3p_\ell d^3p_\nu d^3p_{q_1} d^3p_{q_2} \ldots. \tag{5}$$

  Many of these integrations are reduced by delta functions.

- $f_{n,j}(q, Q^2)$ is the parton distribution function in the proton or antiproton ($n = 1$ or 2, respectively) for the initial state parton associated with configuration j, carrying momentum q, evaluated at the factorization scale Q^2. We use the same scales as used for official Monte Carlo generation. This analysis uses CTEQ6L1 [4] leading-order parton distribution functions via LHAPDF [5].

- $d\sigma_{hs}/dy$ is the differential cross section for the hard scatter collision. It is proportional to the square of the leading order matrix element as given by:

$$d\sigma_{hs} = \frac{(2\pi)^4}{4\sqrt{(q_1 \cdot q_2)^2 - m_1^2 m_2^2}} |\mathcal{M}|^2 d\Phi \tag{6}$$

  where q and m are the four-momenta and masses of the initial state partons.

- $W_j(x, y)$, which can also be written as $W(x \,|\, y, j)$, is called the transfer function. It represents the conditional probability to observe configuration x in the detector given the original parton configuration (y, j). This is divided into two parts:

$$W(x \,|\, y, j) = W_{\rm perm}(x \,|\, y, j)\ W_{\rm reco}(x \,|\, y, j) \tag{7}$$

  where $W_{\rm perm}(x \,|\, y, j)$ is the weight assigned to the given jet-to-parton permutation, and $W_{\rm reco}(x \,|\, y, j)$ relates the reconstructed value to parton values for a given permutation.

- $\Theta_{\rm parton}(y)$ represents the parton level cuts applied in order to avoid singularities in the matrix element evaluation.

VEGAS Monte Carlo integration is used, as implemented in the GNU Scientific Library [8, 9].

The probability to observe a particular event given a process hypothesis, Eq. 1, also requires the total cross section ($\times$ branching faction) as a normalization. Logically, that is just an integration of Eq. 4:

$$\sigma = \int dx\, \frac{d\sigma}{dx}\, \Theta_{\rm reco}(x). \tag{8}$$

The term, $\Theta_{\rm reco}(x)$, approximates the selection cuts. While conceptually simple, this winds up being a huge integral: 13 dimensions for two-jet events, 17 dimensions for three-jet events other than $t\bar{t}$, and 20 dimensions for $t\bar{t}$. However, this integral needs to be calculated only once, not once per event, so the actual integration time is insignificant.

B. The Matrix Elements

The matrix elements used in this analysis are given in Table I. They are taken from the Madgraph [6] leading-order matrix-element generator and use the HELAS [7] routines to evaluate the diagrams. The tqg, $Wcgg$, $Wggg$, and lepjets matrix elements are new to this version of the ME analysis. In the table, for the single top processes, the top quark is understood to decay leptonically: $t \to \ell^+\nu b$, and for the W + jets processes, the W boson is also understood to decay leptonically: $W^+ \to \ell^+\nu$. The charge conjugate processes are also used. The same matrix elements are used for both the electron and muon channels. Furthermore, we use the same matrix elements for heavier generations of incoming quarks, assuming a diagonal CKM matrix. In other words, for the $t\bar{b}$ process, we use the same matrix element for $u\bar{d}$ and $c\bar{s}$ initial state partons.

C. The $t\bar{t}$ Integration

For the $t\bar{t}$→ℓ+jets integration, we cannot assume one-to-one matching of parton to reconstructed object. The final state has four quarks, so one-to-one matching would lead to a four-jet event. We are interested, however, in using the lepjets matrix element in the three-jet bin. The $t\bar{t}$ events therefore have to "lose" one jet to enter this bin. One way that this jet could be lost is by having its reconstructed $p_{\rm T}$ be below our cutoff, which is 15 GeV. A $t\bar{t}$→ℓ+jets event that has a fourth jet with $p_{\rm T} = 13$ GeV, for example, would consider the fourth jet lost. Another way to lose a jet is to merge it with another nearby object. The jet could also be outside the η acceptance of the analysis, which is $|\eta| < 3.4$. There is also general reconstruction inefficiency that could cause a jet to be lost, but that is small.

A study of $t\bar{t}$→e+jets Monte Carlo events before tagging showed that 80 % of the time a jet was lost there was no jet that passed the selection cuts within $\Delta R < 0.5$: it was not merged with another jet. The $p_{\rm T}$ of quarks not matched to a jet passing the selection cuts is peaked at around 15 GeV, suggesting that the jet is often lost because

The Matrix Elements

Two Jets		Three Jets	
Name	Process	Name	Process
tb	$u\bar{d} \to t\bar{b}$ (1)	tbg	$u\bar{d} \to t\bar{b}g$ (5)
tq	$ub \to td$ (1)	tqg	$ub \to tdg$ (5)
	$\bar{d}b \to t\bar{u}$ (1)		$\bar{d}b \to t\bar{u}g$ (5)
		tqb	$ug \to td\bar{b}$ (4)
			$\bar{d}g \to t\bar{u}\bar{b}$ (4)
Wbb	$u\bar{d} \to Wb\bar{b}$ (2)	$Wbbg$	$u\bar{d} \to Wb\bar{b}g$ (12)
Wcg	$\bar{s}g \to W\bar{c}g$ (8)	$Wcgg$	$\bar{s}g \to W\bar{c}gg$ (54)
Wgg	$u\bar{d} \to Wgg$ (8)	$Wggg$	$u\bar{d} \to Wggg$ (54)
		lepjets	$q\bar{q} \to t\bar{t} \to \ell^+\nu b\bar{u}d\bar{b}$ (3)
			$gg \to t\bar{t} \to \ell^+\nu b\bar{u}d\bar{b}$ (3)

TABLE I: The Matrix Elements used in the analysis are given. The number in parenthesis specifies the number of Feynman diagrams included in the process. For simplicity, only the processes that contain a positively-charged lepton in the final state are shown. The charge conjugated processes are also used.

it falls below the jet p_{T} threshold. The study showed that the light quark jets, which have a softer p_{T} spectrum, were 1.7 times as likely to be lost (not by merging) as the heavy quarks. This observation motivated us to make the following simplification: assume that it is a light quark coming from the hadronically-decaying W that is lost. In the usual case, the probability assigned to losing a jet is the probability that the jet is reconstructed to have $p_{\mathrm{T}} < 15\,\mathrm{GeV}$, which can be calculated from the transfer functions. Other special cases considered are when the two light quarks overlap, in which case they are assumed to merge, or if the η of the jet is outside our acceptance.

D. Assignment Permutations

As mentioned before, Eq. 7 incorporates the (discrete) summation over different configurations, which includes the summation over the different ways to assign the partons to the jets. A weight for each permutation is included as the W_{perm} part of the transfer function. This analysis uses two pieces of information to determine the weight, namely b-tagging and muon charge:

$$W_{\mathrm{perm}} = W_{b\mathrm{tag}} W_{\mu\mathrm{charge}}. \tag{9}$$

The b-tagging weight is assumed to factor by jet:

$$W_{b\mathrm{tag}} = \prod_i w_{b\mathrm{tag}}(\mathrm{tag}_i \,|\, \alpha_i, p_{\mathrm{T}i}, \eta_i), \tag{10}$$

where α_i is the flavor of quark i and tag_i is true or false depending on whether the jet is tagged or not. The weights assigned to cases with and without a b-tag are:

$$w_{b\mathrm{tag}}(\mathrm{tag} = \mathrm{true} \,|\, \alpha, p_{\mathrm{T}}, \eta) = P^{\mathrm{taggable}}(p_{\mathrm{T}}, \eta)\varepsilon_\alpha(p_{\mathrm{T}}, \eta) \tag{11}$$

$$w_{b\mathrm{tag}}(\mathrm{tag} = \mathrm{false} \,|\, \alpha, p_{\mathrm{T}}, \eta) = 1 - P^{\mathrm{taggable}}(p_{\mathrm{T}}, \eta)\varepsilon_\alpha(p_{\mathrm{T}}, \eta), \tag{12}$$

where ε_α is the tag-rate function for the particular quark flavor and P^{taggable} is the taggability-rate function, which is the probability that a jet is taggable.

For the s-channel matrix element and for the lepjets matrix element, there is both a b-quark and a $\bar{b}$-quark in the final state. Furthermore the matrix element is not symmetric with respect to the interchange of the b and $\bar{b}$ quarks, so it would be useful to be able to distinguish between b-jets and $\bar{b}$-jets to make the correct assignment. In the case of muonic decays of the b or $\bar{b}$ quark, it is possible to distinguish between the jets by the charge of the decay muon. One complication is that a charm quark may also decay muonically, and the charge of the muon differs between $b \to c\mu^-\nu$ and $b \to cX\bar{X}' \to s\mu^+\bar{\nu}X\bar{X}'$. However, because $p_{\mathrm{T_{rel}}}$, the muon p_{T} relative to the jet axis, differs in the two case, the charge of the muon still provides information, and $W_{\mu\mathrm{charge}}$ is calculated in a manner similar to $W_{b\mathrm{tag}}$.

E. Single Top Discriminant

The form of the discriminant was given in Eq. 3. A natural question is which matrix elements are used in "signal" and which in "background." We build separate s-channel and t-channel discriminants, D_s and D_t. Looking at Table I, there is only one s-channel matrix element considered per channel, so that is the one that is used in $P(x|\text{signal})$ to build D_s for that particular channel. When building D_t for two-jet events, both processes labeled tq are added when calculating the matrix element. By analogy, when building D_t for three-jet events, all the processes in both tqg and tqb are logically added:

$$P(x\,|\,3\text{jet}, t\text{channel}) = \frac{1}{(\sigma_{tqb}+\sigma_{tqg})}\frac{d(\sigma_{tqb}+\sigma_{tqg})}{dx}. \tag{13}$$

This can also be written as:

$$\begin{aligned} P(x\,|\,3\text{jet}, t\text{channel}) &= \frac{\sigma_{tqb}}{(\sigma_{tqb}+\sigma_{tqg})}\frac{1}{\sigma_{tqb}}\frac{d\sigma_{tqb}}{dx} + \frac{\sigma_{tqg}}{(\sigma_{tqb}+\sigma_{tqg})}\frac{1}{\sigma_{tqg}}\frac{d\sigma_{tqg}}{dx} & (14)\\ &= w_{tqb}P(x|tqb) + w_{tqg}P(x|tqg), & (15)\end{aligned}$$

where w_{tqb} and w_{tqg} are the relative yields of the two signal processes based on the yield fractions calculated in each case, i.e., the normalization cross section calculated as given by Eq. 8. We decided to keep the same methodology of using weights based on yield fraction for the $P(x|\text{background})$ calculations, but instead of using the normalization cross section, we use the yield fraction of the official MC samples, because some matrix elements are meant to handle a class of backgrounds, not just the exact process it represents.

The performance of the s-channel and t-channel discriminants can be seen in Fig. 1. These are plots of the fraction of s-channel (t-channel) signal that passes versus the fraction of background that passes, varying the cut value c in $D_s > c$ ($D_t > c$), for various backgrounds.

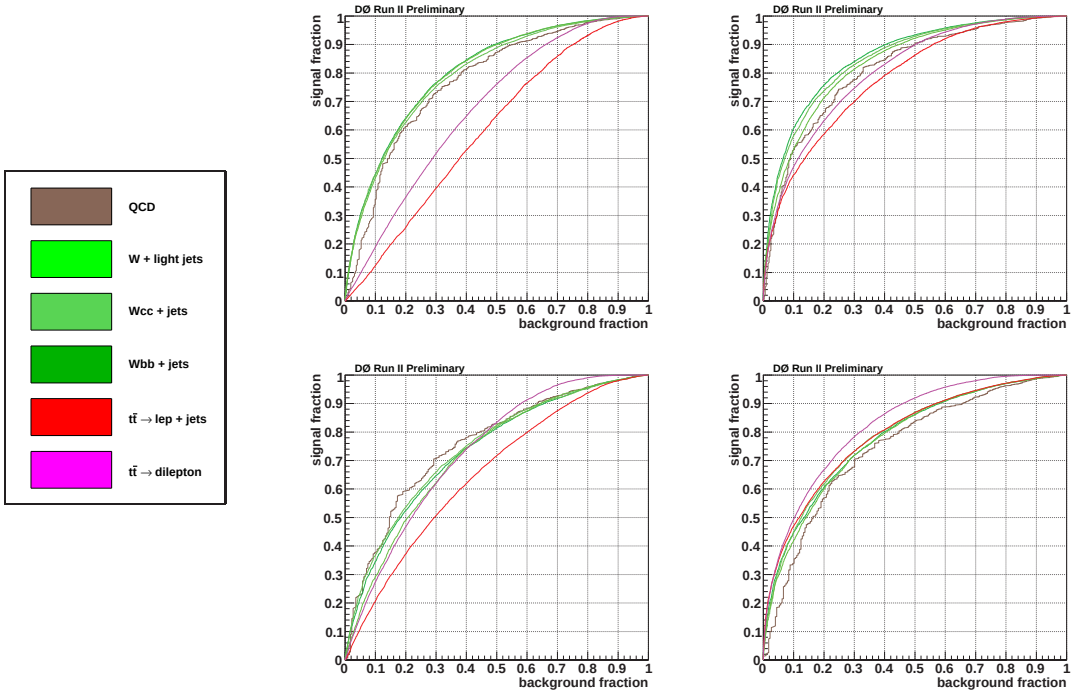

FIG. 1: Discriminant performance in the e+jets one b-tag channel vs. various backgrounds, with the legend specifying the background. Left is the D_s performance, right the D_t performance, for two-jet (upper row) and three-jet (lower row) events.

III. CROSS-CHECK SAMPLES

An important step in the single top search is to establish that the background model is appropriate while minimizing sampling the search region. For this purpose, two background-dominated control samples are defined to consist of

events that pass the standard event selection and in addition $H_{\rm T} < 175$ GeV or $H_{\rm T} > 300$ GeV. We call these control samples "soft W+jets" and "hard W+jets" respectively because two-jet events are largely dominated by W+jets background, and these cross-checks mainly test the modeling of that background. In the case of three-jet events, the "hard W+jets" sample also contains a significant fraction of $t\bar{t}$.

Fig. 2 compares the discriminants between data and the background model for the "soft W+jets" sample, and Fig 3 does the same for the "hard W+jets" sample. The single top quark content is scaled to the measured cross section. Good agreement is seen.

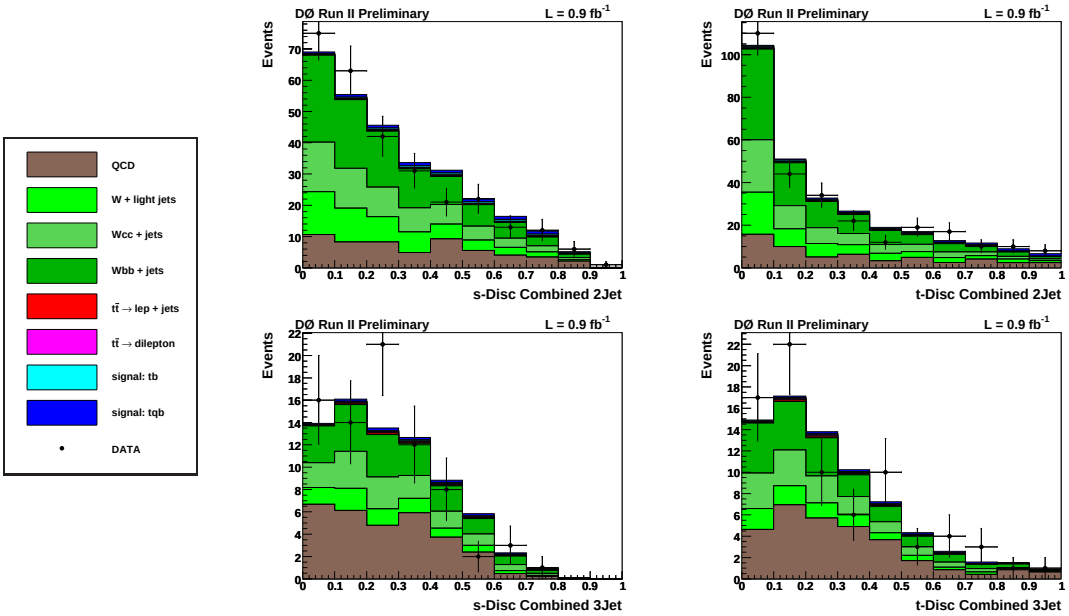

FIG. 2: "Soft W+jets" cross-check plots in two-jet (upper row) and three-jet (lower row) events for the s-channel discriminant (left) and the t-channel discriminant (right).

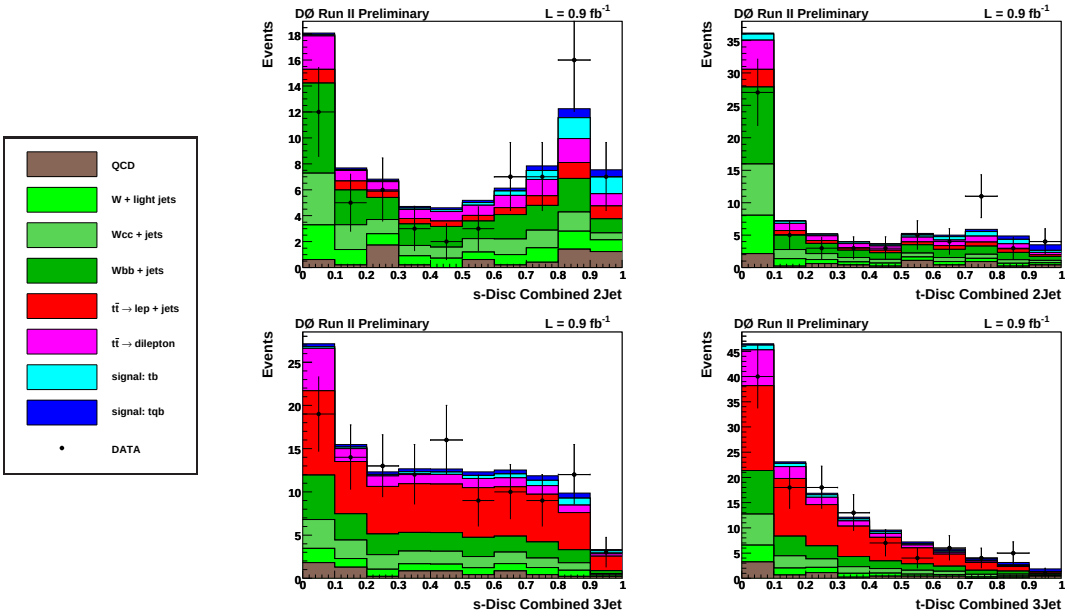

FIG. 3: "Hard W+jets" cross-check plots in two-jet (upper row) and three-jet (lower row) events for the s-channel discriminant (left) and the t-channel discriminant (right).

IV. CALIBRATION

Several ensembles of simulated data sets were produced from the background model to test the calibration of the method. They were generated with a non-SM $tb+tqb$ cross section but with the tb:tqb cross section ratio fixed at the SM value ($\sigma_s/\sigma_t = 0.44$). The fitted function is $\sigma_{\rm meas} = 0.95\sigma_{\rm in} + 0.46\,{\rm pb}$ with $\chi^2/{\rm ndof} = 2.73/2$.

V. EXPECTED RESULTS

Setting the number of observed events to be equal to the expected (SM) signal plus the expected background gives us the expected performance. Table II shows the expected cross sections for various combinations of analysis channels, and Fig. 4 shows the tb+tqb posterior for the combination of all channels. The expected result for each combination is consistent with the Standard Model cross section of 2.9 pb that we used.

Expected tb+tqb Cross Section						
1,2tags + 2,3jets		e,μ + 2,3jets		e,μ + 1,2tags		All
e-chan	μ-chan	1 tag	2 tags	2 jets	3 jets	channels
$2.7^{+2.0}_{-1.7}$	$2.9^{+2.3}_{-2.0}$	$2.8^{+1.7}_{-1.5}$	$2.7^{+3.3}_{-2.6}$	$2.8^{+1.8}_{-1.6}$	$2.9^{+2.7}_{-2.3}$	$\mathbf{2.8^{+1.6}_{-1.4}}$

TABLE II: Expected tb+tqb cross sections for many combinations of the analysis channels. The final expected result of this analysis are shown in bold type.

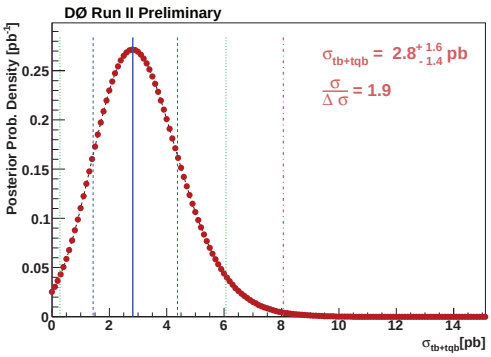

FIG. 4: Expected 1D posterior plots for all channels combined.

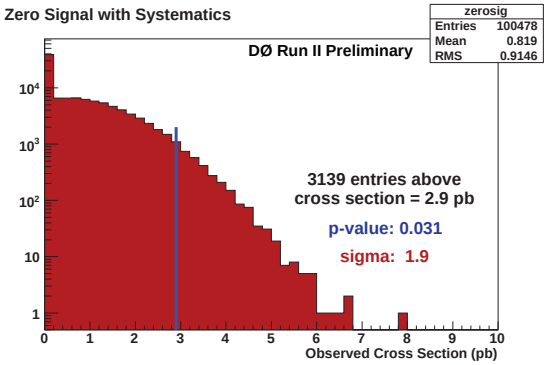

FIG. 5: Distribution of cross sections from a zero-signal ensemble and expected p-value using $\sigma = 2.9$ pb.

A measure of the significance of our measurement is the probability that the background alone could fluctuate up to or above the measured cross section. Figure 5 shows the distribution of measured cross sections for an ensemble made up of simulated zero-signal data sets. The data sets had both statistical and systematic variations applied when they were created. From this distribution, we calculate a p-value of 3.1% assuming there is Standard Model single-top with $\sigma = 2.9$ pb, meaning that only 3.1% of the time zero signal could cause the ME method to measure $\sigma \geq 2.9$ pb. This corresponds to a 1.9σ Gaussian-equivalent significance.

VI. OBSERVED RESULTS

A. Discriminant Output

Fig. 6 and Fig. 7 show the s-channel and t-channel discriminant histograms for two-jet and three-jet events. The different lepton and number of b-tags channels are combined here for illustration purposes. The single top quark content is scaled to the measured cross section.

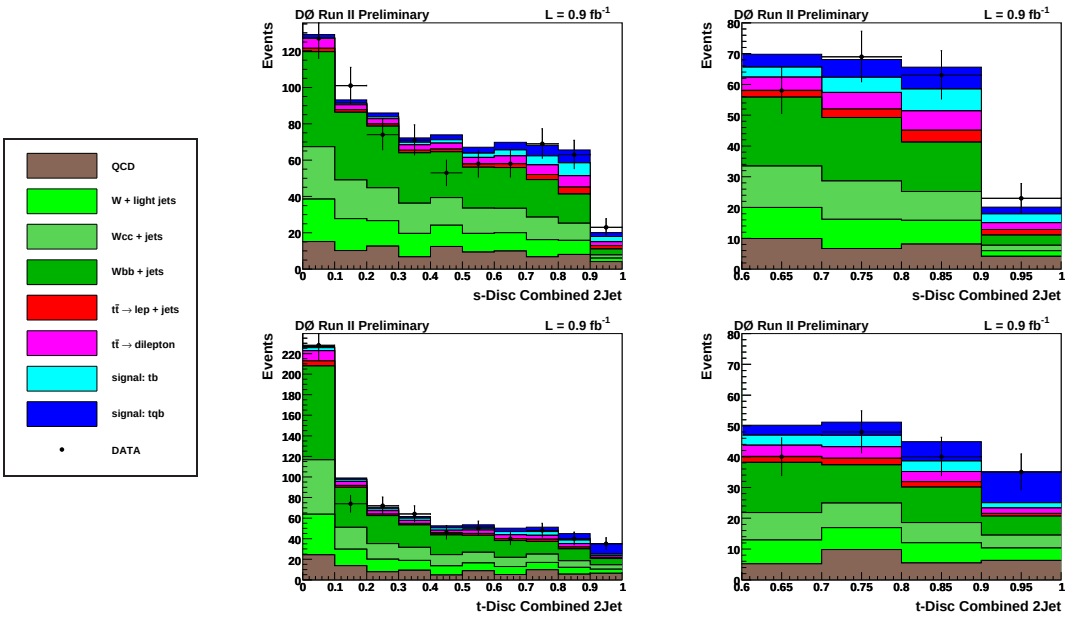

FIG. 6: Discriminant results for the e+μ channel with two jets and ≥ 1 b tag. Upper row: s-channel discriminant; lower row: t-channel discriminant. Left column: full output range; right column: close-up of the high end of the distributions.

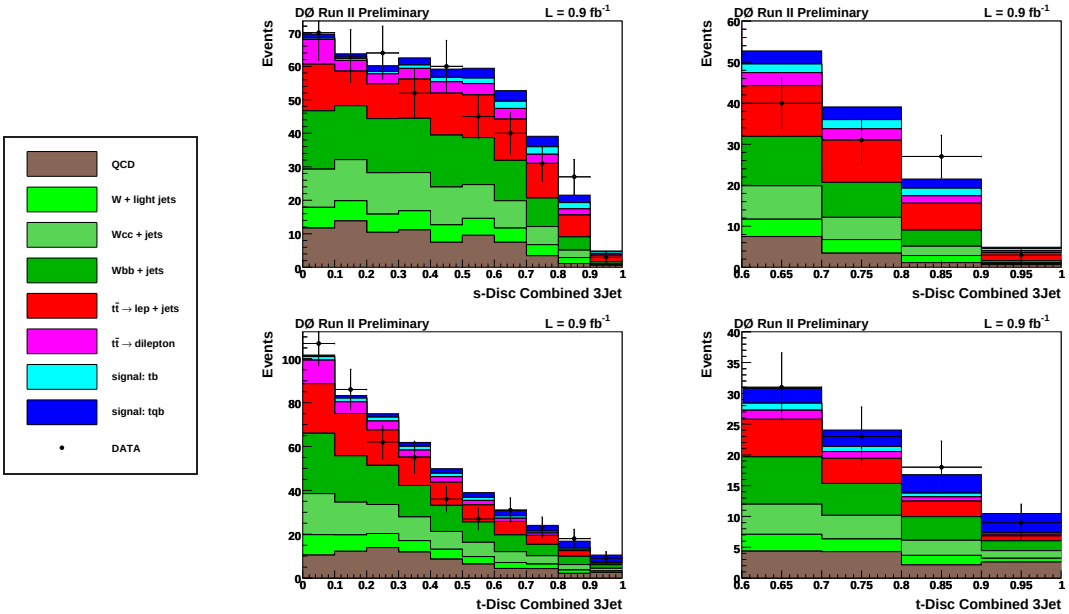

FIG. 7: Discriminant results for the e+μ channel with three jets and ≥ 1 b tag. Upper row: s-channel discriminant; lower row: t-channel discriminant. Left column: full output range; right column: close-up of the high end of the distributions.

B. Measured Cross Section

Table III shows the measured cross sections from various combinations of analysis channels, and Fig. 8 shows the observed tb+tqb posterior for all channels combined. The combined result with full systematics is:

$$\sigma\left(p\bar{p} \rightarrow tb + tqb + X\right) = 4.8^{+1.6}_{-1.4}\ \text{pb}.$$

This result assumes a Standard Model cross section ratio of $\sigma_s/\sigma_t = 0.44$.

Measured tb+tqb Cross Section						
1,2tags + 2,3jets		e,μ + 2,3jets		e,μ + 1,2tags		All
e-chan	μ-chan	1 tag	2 tags	2 jets	3 jets	channels
$4.3^{+2.0}_{-1.7}$	$5.9^{+2.6}_{-2.2}$	$4.6^{+1.8}_{-1.5}$	$7.5^{+4.3}_{-3.5}$	$5.1^{+2.0}_{-1.7}$	$4.4^{+2.7}_{-2.2}$	$\mathbf{4.8^{+1.6}_{-1.4}}$

TABLE III: Measured tb+tqb cross sections for many combinations of the analysis channels. The final result of this analysis is shown in bold type.

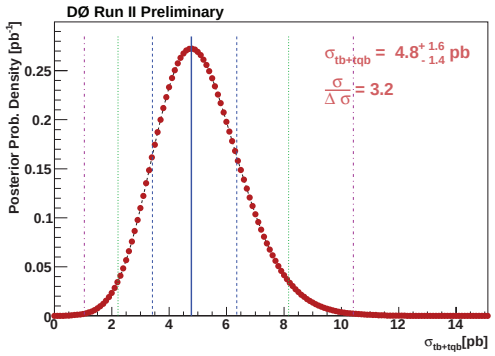

FIG. 8: Measured 1D posterior plots for all channels combined.

C. Signal Significance

Fig. 9 on the left shows the same distribution of measured cross sections for an ensemble made up of simulated zero-signal data sets as Fig. 5. Using the measured cross section of 4.8 pb, from this distribution, we calculate a p-value of 0.08%, meaning that only 0.08% of the time zero signal could cause the ME method to measure $\sigma \geq 4.8$ pb. That corresponds to a 3.2σ Gaussian-equivalent significance. Fig. 9 on the right shows the distribution of measured cross sections for an ensemble made up of simulated Standard Model signal (2.9 pb) data sets. This ensemble also has full systematics included. From this distribution, we calculate a p-value of 13%, meaning that 13% of the time a Standard Model signal could cause the ME method to measure $\sigma \geq 4.8$ pb, corresponding to 1.1σ.

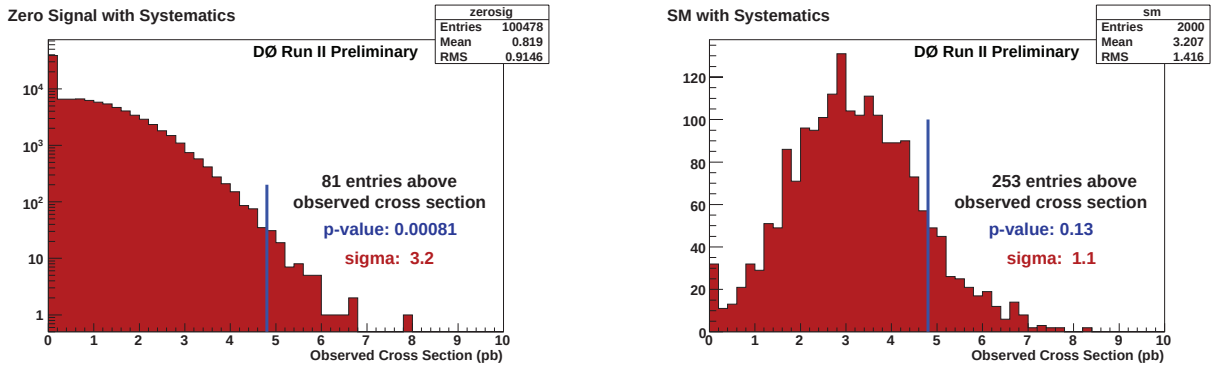

FIG. 9: Distribution of cross sections from a zero-signal ensemble (left) and a Standard Model ensemble (right) with full systematics included.

VII. EVENT CHARACTERISTICS

As a test to see if the discriminant really does find single-top events, we plot the distributions of variables after applying a cut on the discriminant value. One variable that has a distinct shape for t-channel single-top events is "$Q \times \eta$," or to be more specific, the charge of the lepton times the pseudorapidity of the untagged jet. It is also expected that the invariant mass of the lepton, $\not\!\!E_{\rm T}$, and b-tagged jet be consistent with the top quark mass. Fig. 10 shows these two variables for different t-channel discriminant cuts. Fig. 11 shows the same variables for different s-channel discriminant cuts. The "$Q \times \eta$" variable does not have the distinct shape, but the invariant mass is again consistent with the top quark mass. In all plots, the single top quark content is scaled to the measured cross section.

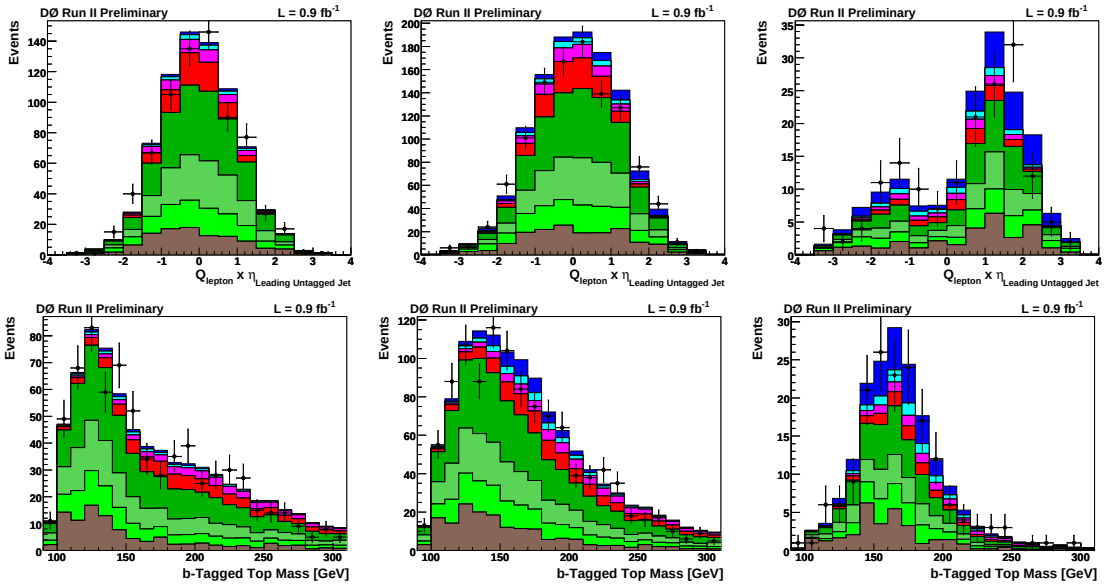

FIG. 10: The upper plots are the lepton charge times the pseudorapidity of the untagged jet, and the lower plots are the invariant mass of the lepton, $\not\!\!E_{\rm T}$, and tagged jet for all events combined. The left plots have $D_t < 0.4$ t-channel discriminant cut. The middle plots include all bins. The right plots have a $D_t > 0.7$ t-channel discriminant cut.

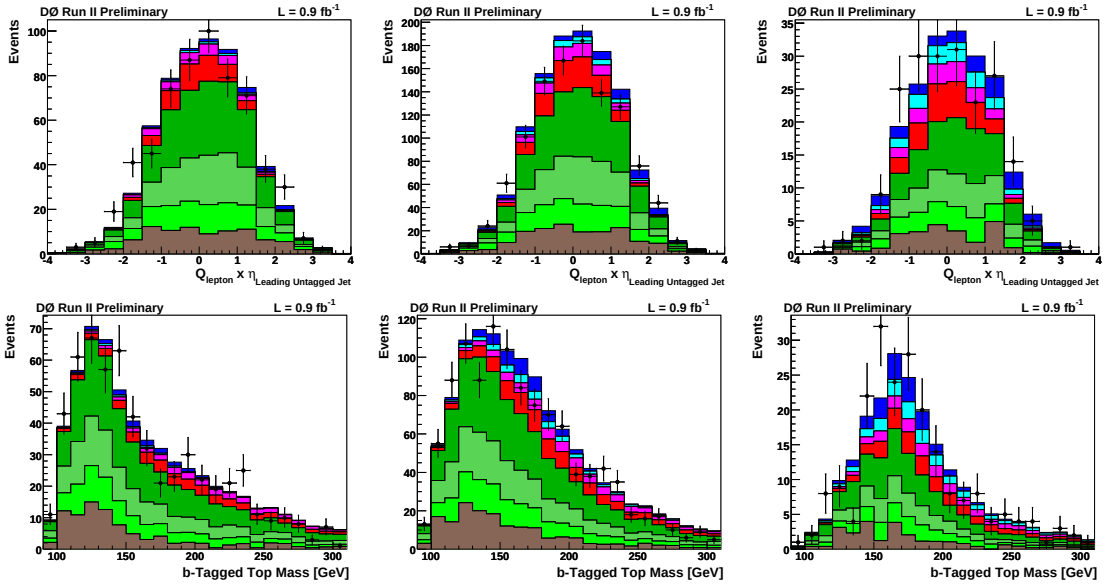

FIG. 11: The upper plots are the lepton charge times the pseudorapidity of the untagged jet, and the lower plots are the invariant mass of the lepton, $\not\!\!E_{\rm T}$, and tagged jet for all events combined. The left plots have $D_s < 0.4$ s-channel discriminant cut. The middle plots include all bins. The right plots have a $D_s > 0.7$ s-channel discriminant cut.

VIII. SUMMARY AND CONCLUSIONS

We have used the matrix elements method to separate single top quark processes from background processes in 0.9 fb^{-1} of Run II data. Assuming a Standard Model cross section ratio of $\sigma_s/\sigma_t = 0.44$, we measure:

$$\sigma\left(p\bar{p} \rightarrow tb + tqb + X\right) = 4.8^{+1.6}_{-1.4} \text{ pb}.$$

This result has a p-value of 0.08%, corresponding to a 3.2σ Gaussian-equivalent significance.

[1] V. M. Abazov *et al.* [D0 Collaboration], "Evidence for production of single top quarks and first direct measurement of |V(tb)|," Phys. Rev. Lett. **98**, 181802 (2007) [arXiv:hep-ex/0612052].

[2] D0 Collaboration, "Evidence for production of single top quarks and first direct measurement of $|V_{tb}|$" `http://www-d0.fnal.gov/Run2Physics/top/public/fall06/singletop/`

[3] I. Bertram *et al.*, "A recipe for the construction of confidence limits," Fermilab-TM-2104 (2000).

[4] J. Pumplin, D. R. Stump, J. Huston, H. L. Lai, P. Nadolsky and W. K. Tung, "New generation of parton distributions with uncertainties from global QCD analysis," JHEP **0207**, 012 (2002) [arXiv:hep-ph/0201195].

[5] The Les Houches Accord PDF Interface, `http://hepforge.cedar.ac.uk/lhapdf/`

[6] F. Maltoni and T. Stelzer, "MadEvent: automatic event generation with MadGraph," JHEP **0302**, 027 (2003).

[7] H. Murayama, I. Watanabe and K. Hagiwara, "HELAS: HELicity amplitude subroutines for Feynman diagram evaluations," KEK-91-11 (1992).

[8] G.P. Lepage, "VEGAS: an adaptive multidimensional integration program," Cornell Laboratory of Nuclear Sciences report CLNS-80/447 (1980).

[9] The GNU scientific library, `http://www.gnu.org/software/gsl/`